Belief Rule Base Modeling Method with Rule Adaptation and Uncertainty Representation for Fault Diagnosis

Dongyang Liu[1], Jun Tao[1], Tianhong Pan[1*]
[1*]School of Electrical Engineering and Automation, Anhui University,
Hefei, 230601, Anhui, China. E-mail(s): thpan@ahu.edu.cn

Abstract: To address the challenges of rule explosion and the representation of expert knowledge uncertainty in traditional Belief Rule Base (BRB) models for complex system fault diagnosis, an adaptive model construction method based on reinforcement learning is proposed in this work. First, a Deep Q-Network (DQN) mechanism is designed to adaptively adjust attribute reference values based on input data, thereby reducing redundancy and mitigating rule explosion. Second, a power set identification framework is introduced, incorporating belief variance and entropy into the parameter optimization process to capture the multidimensional uncertainty inherent in expert knowledge. Furthermore, a dimensionality reduction and clustering analysis method based on the rule activation weight matrix is presented to systematically evaluate the impact of reference value adjustments on model structure and inference performance. Finally, experimental results demonstrate that the proposed method significantly enhances the structural compactness, inference robustness, and predictive accuracy of BRB models in uncertain and complex environments.

Key-Words: *belief rule base, fault diagnosis, expert knowledge, reinforcement learning, power set.*

1. Introduction

In modern industrial production and engineering applications, complex systems are widely deployed in critical domains such as power systems, aerospace, and fundamental physics due to their characteristics of strong coupling, nonlinearity, multivariable interactions, and time-varying behavior. However, failures in such systems may lead to severe economic losses and safety hazards. Therefore, implementing effective Fault Diagnosis (FD) has become a critical task to ensure the reliability and safety of complex systems [1].

Fault diagnosis approaches for complex systems can be broadly categorized into three types based on modelling strategy and knowledge dependency: (1) Data-driven methods, which learn directly from data using models such as neural networks [2]. These methods capture nonlinear patterns but often suffer from poor interpretability and sensitivity to data quality [3]. (2) Mechanism-based methods, which rely on physical knowledge or expert rules and provide high interpretability [4], but lack adaptability in complex systems, fuzzy logic-based detection [5] and fault-tree analysis [6]. (3) Knowledge–data fusion methods, represented by the Belief Rule Base (BRB) framework [7], which integrates numerical data and expert rules for robust reasoning under uncertainty. Existing enhancements include interval-valued belief degrees [8] and hybrid BRB models [9].

Despite its strengths, BRB faces two core challenges: rule explosion, where rule count grows exponentially, and expert knowledge uncertainty, which affects inference reliability. Recent studies explored

Received: 2025/11/20, Accepted: 2025/12/28
*Corresponding author: Tianhong Pan
E-mail address: thpan@ahu.edu.cn

interval BRB with rule reliability [10], OR-type BRB structures [11], and interpretability improvements [12], but limitations remain in scalability and optimization efficiency.

To address these issues, this paper proposes an adaptive modeling framework that integrates deep reinforcement learning with a power-set-based BRB optimization strategy. The main contributions are:

1) A Deep Q-Network (DQN)-based reinforcement learning mechanism is developed to dynamically adjust the reference values of attributes according to input data, reducing redundant rules and mitigating rule explosion.

2) A power-set inference framework is introduced with belief variance and entropy integrated into inference and optimization, enabling multi-dimensional uncertainty characterization under incomplete and ambiguous expert knowledge.

3) A rule-activation-matrix-based dimensionality reduction and clustering method is proposed to quantify the impact of reference value adjustment, demonstrating improved rule activation efficiency and a simplified inference structure.

2. Basic knowledge of PBRB

2.1 Description of PBRB

The PBRB model incorporates a power-set–based inference mechanism to reduce expert-knowledge uncertainty [13]. The kth rule is expressed as:

$$\begin{aligned} &R_k: \textit{If } x_1 \textit{ is } A_1^k \wedge x_2 \textit{ is } A_2^k \text{L} \wedge x_M \textit{ is } A_M^k, \\ &\quad \textit{then } y \textit{ is } \left\{\left(\phi_1,\beta_{1,k}\right),\text{L},\left(\phi_{N+1},\beta_{N+1,k}\right),\text{L},\left(\phi_{2^N},\beta_{2^N,k}\right)\right\}, \\ &\quad \textit{with rule weight } \theta_k, \\ &\quad \textit{antecedent attribute weight } \delta_1,\delta_2,\text{L},\delta_M, \\ &\quad \left(\sum_{n=1}^{2^N}\beta_{n,k}\le 1\right), k\in\{1,2,\text{L},L\}, \end{aligned} \tag{1}$$

where x_1,L,x_M are the input attributes, A_1^k,L,A_M^k are the reference values for rule k. y is the output of the PBRB model. The power set recognition framework expands these into 2^N output results, that is $\left\{\phi_1,\text{L},\phi_{2^N}\right\}$. The belief degrees $\left\{\beta_{1,k},\text{L},\beta_{2^N,k}\right\}$ represent the credibility assigned to each output subset. A belief degree assigned to a singleton such as $\left(D_1,D_2\right),\text{L},\left(D_2,\text{L},D_N\right)$ represents local certainty, $\left(D_1,\text{L},D_N\right)$ represents global uncertainty [14]. The rule weight θ_k reflects rule importance, while $\delta_1,\text{L},\delta_M$ denote attribute weights.

2.2 Reasoning in PBRB

Step 1: Input transformation

Transform the input information of different attributes into belief distributions over the reference values. The matching degree is calculated as follows:

$$\alpha_{i,j}^k=\begin{cases}\dfrac{A_{i(l+1)}^k-x_i}{A_{i(l+1)}^k-A_{il}^k}, & j=l,\ (A_{il}^k\le x_i\le A_{i(l+1)}^k),\\ \dfrac{x_i-A_{il}^k}{A_{i(l+1)}^k-A_{il}^k}, & j=l+1,\ (A_{il}^k\le x_i\le A_{i(l+1)}^k),\\ 0, & else,\end{cases} \tag{2}$$

where $\alpha_{i,j}^k$ denotes the matching degree, A_{il}^k and $A_{i(l+1)}^k$ are the lth and $(l+1)th$ reference values of the ith attribute in the kth rule [15].

Step 2: Calculation of activation weights

Each rule activation weight ω_k is determined:

$$\omega_k=\frac{\theta_k\alpha_k}{\sum_{i=1}^{L}\theta_i\alpha_i} \tag{3}$$

where ω_k denotes the activation weight, $k=1,\cdots,L$, and θ_k represents the rule weight. α_k is the overall matching degree of the kth belief rule, and it is calculated using the following formula:

$$\boldsymbol{\alpha}_k=\prod_{i=1}^{M}\left(\boldsymbol{\alpha}_{i,j}^k\right)^{\overline{\delta}_i} \tag{4}$$

$$\overline{\delta}_i=\frac{\delta_i}{\max\limits_{m=1,2\text{L},M}\{\delta_m\}} \tag{5}$$

where $\overline{\delta}_i$ represents the normalized relative weight, δ_i denotes the original weight of the input attribute assigned, M is the total number of input attributes.

Step 3: Fusion of the belief rule base

To reduce computational complexity, the analytical ER formulation is used [14]:

$$\beta_n = \frac{\mu\left[\prod_{k=1}^{L}\left(\omega_k\beta_{n,k}+1-\omega_k\sum_{j=1}^{2^N-1}\beta_{j,k}\right)-\prod_{k=1}^{L}\left(1-\omega_k\sum_{j=1}^{2^N-1}\beta_{j,k}\right)\right]}{1-\mu\left[\prod_{k=1}^{L}(1-\omega_k)\right]}, \quad (6)$$

$$\mu=\left[\sum_{n=1}^{N}\prod_{k=1}^{L}\left(\omega_k\beta_{n,k}+1-\omega_k\sum_{j=1}^{2^N-1}\beta_{j,k}\right)-(N-1)\prod_{k=1}^{L}\left(1-\omega_k\sum_{j=1}^{2^N-1}\beta_{j,k}\right)\right]^{-1} \quad (7)$$

where β_n denotes the belief degrees of the consequents $\phi_n\left(n=1,\mathrm{L}\ ,2^N-1\right)$, excluding the empty set, μ denotes normalized intermediate variable.

3. Reference values adjustment and optimization modeling

3.1 Reinforcement learning environment

An eight-dimensional state vector s_i is designed to describe the model's structure and behavior:

$$s_i=\left(v_{i,1},v_{i,2},w_{i,1},w_{i,2},k_i,y_i\right) \quad (8)$$

where $v_{i,1},v_{i,2}$ are the number of reference values for each attribute, and $w_{i,1},w_{i,2}$ denote the interval coverage, k_i is the number of rules and y_i is the inference output.

The action space is defined as a two-dimensional discrete set:

$$a_i^1=(t_{i,1}^1,t_{i,2}^1,t_{i,3}^1,t_{i,4}^1,t_{i,5}^1,t_{i,1}^2,t_{i,2}^2,t_{i,3}^2,t_{i,4}^2,t_{i,5}^2) \quad (9)$$

$$a_i^2=(p_{i,1},p_{i,2},\ldots,p_{i,k},v_{i,1},v_{i,2},\ldots,v_{i,k}) \quad (10)$$

where $t_{i,1},t_{i,2},t_{i,3},t_{i,4},t_{i,5}$ denote the five structural operations, $p_{i,k}$ denotes the indices of the reference values, $v_{i,k}$ is corresponding adjustment magnitudes.

The reward r_i^1 is defined to guide the PBRB structure optimization, the r_i^2 is an improvement reward during the continuous adjustment phase:

$$r_i^1=-\left(s_{i,5}+\lambda s_{i,6}\right) \quad (11)$$

$$r_i^2=clip\left[\left(s_{i-1,5}-s_{i,5}\right),-1,1\right] \quad (12)$$

where λ is the structural complexity penalty.

The theoretical framework of the DQN algorithm is shown in Fig.1.

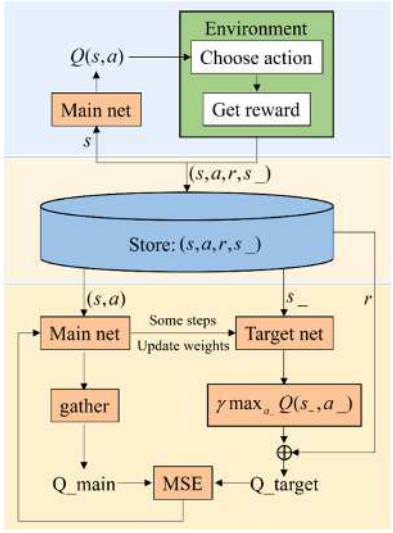

Fig.1 Schematic diagram of the DQN

3.2 Multidimensional uncertainty modeling

To evaluate the uncertainty of local and global ignorance, two metrics are employed: (1) Belief variance: Indicates the degree of concentration of a belief distribution for a single rule; (2) Entropy: Measures the overall dispersion and disorder in the rule base inference outcomes. The variance V^k and entropy E^k are computed as:

$$V^k=\frac{1}{2^N-1}\sum_{n=1}^{2^N-1}\left(\beta_{n,k}-\overline{\beta}_{n,k}\right)^2 \quad (13)$$

$$E^k=-\sum_{n=1}^{2^N-1}\beta_{n,k}\log\beta_{n,k} \quad (14)$$

Define the mean square error MSE^k of $y(i)$ and $\hat{y}(i)$, $y(i)$ is the inference output according to utility theory.

A weighted multi-objective optimization function is designed to balance predictive accuracy and uncertainty reduction:

$$\begin{aligned}&\min F(\theta_k,\delta_i,\beta_{n,k})=\lambda_1\frac{MSE^k}{\max(MSE^k)}-\lambda_2\frac{V^k}{\max(V^k)}+\lambda_3\frac{E^k}{\max(E^k)}\\&s.t.\ \ 0\le\beta_{n,k}\le1,\ n=1,\mathrm{L}\ ,2^N-1,\ k=1,\mathrm{L}\ ,L,\\&\quad\sum_{n=1}^{2^N-1}\beta_{n,k}\le1,\\&\quad0\le\theta_k\le1,\ k=1,\mathrm{L}\ ,L,\\&\quad0\le\delta_i\le1,\ i=1,\mathrm{L}\ ,M,\end{aligned} \quad (15)$$

where $\max(MSE^k),\max(V^k),\max(E^k)$ correspond to the maximum values of the MSE, belief variance, and entropy. $\lambda_1,\lambda_2,\lambda_3$ are weighting factors set.

3.3 Structure interpretability assessment

In the inference process of the PBRB, an activation weight matrix W is constructed:

$$W=\begin{bmatrix} \omega_{11} & \omega_{12} & \mathrm{L} & \omega_{1L} \\ \omega_{21} & \omega_{22} & \mathrm{L} & \omega_{2L} \\ \mathrm{M} & \mathrm{M} & \mathrm{O} & \mathrm{M} \\ \omega_{T1} & \omega_{T2} & \mathrm{L} & \omega_{TL} \end{bmatrix} \tag{16}$$

Three quantitative indicators are introduced:

1) The mean rule correlation $\bar{\rho}$ is used to measure redundancy among rules:

$$\bar{\rho}=\frac{2}{L(L-1)}\sum_{i<j}\frac{W_{:,i}W_{:,j}}{\left\|W_{:,i}\right\|\left\|W_{:,j}\right\|} \tag{17}$$

where $W_{:,i}$ denotes the activation vector of rule i across all samples, and $W_{:,j}$ represents that of rule j.

2) The mean activation entropy $\tilde{H}$ of each rule's is defined as [16]:

$$\tilde{H}=-\frac{1}{T\log L}\sum_{t=1}^{T}\sum_{k=1}^{L}p_k^t\log p_k^t \tag{18}$$

where p_k^t denotes the normalized activation probability of rule k for sample t.

3) The clustering separability D is calculated as:

$$D=\frac{1}{K}\sum_{i=1}^{K}\max_{i\neq j}\frac{\sigma_i+\sigma_j}{d_{ij}} \tag{19}$$

where K is the number of clusters, σ_i denotes the average intra-cluster distance of cluster i, and d_{ij} is the centroid distance between clusters i and j.

4. Case study

A real pipeline-leakage dataset is used. The dataset includes 2,008 samples collected every 10 seconds from flow and pressure sensors under normal and controlled-leak conditions. Leak events can be identified by inlet–outlet flow discrepancies and abnormal pressure variations. Thus, the *FlowDiff* and *PressureDiff* are selected as antecedent attributes, and the *LeakSize* serves as the consequent attribute.

4.1 Training and testing of the proposed model

Combining operating data and expert knowledge, leaks are identified by inlet–outlet flow discrepancies and abnormal pressure changes.

After adaptive adjustment, the number of reference values for the *FlowDiff* is reduced from 8 to 7, and that for the *PressureDiff* is reduced from 7 to 6, resulting in a more compact rule base of 42 rules. The optimized model parameters are presented in Table 1.

Table 1 Optimized PBRB model by training

No	δ_1	δ_2	θ_k	$\{L,M,H,(L,M),(L,H),(M,H),(L,M,H)\}$
1	NL	NL	0.5064	(0.1496, 0.1879, 0.2020, 0.1254, 0.0209, 0.0553, 0.2589)
2	NL	NM	0.6811	(0.0742, 0.1556, 0.6934, 0.0017, 0.0135, 0.0149, 0.0467)
3	NL	NS	0.1871	(0.0505, 0.0568, 0.6851, 0.0298, 0.0717, 0.0000, 0.1061)
4	NL	PS	0.2842	(0.0435, 0.5532, 0.0132, 0.0403, 0.0943, 0.0616, 0.1939)
5	NL	PM	0.1577	(0.0160, 0.4372, 0.3018, 0.0372, 0.1349, 0.0265, 0.0464)
6	NL	PL	0.9079	(0.3647, 0.2104, 0.0026, 0.0123, 0.2013, 0.0704, 0.1383)
7	NM	NL	0.3234	(0.3918, 0.1949, 0.0042, 0.0000, 0.3157, 0.0889, 0.0045)
8	NM	NM	0.7712	(0.0005, 0.3257, 0.1911, 0.0578, 0.0288, 0.3872, 0.0089)
9	NM	NS	0.3779	(0.0452, 0.1315, 0.3125, 0.0678, 0.1096, 0.0965, 0.2369)
10	NM	PS	0.5040	(0.0745, 0.4973, 0.0088, 0.0493, 0.2290, 0.1127, 0.0284)
11	NM	PM	0.9315	(0.0007, 0.4228, 0.0086, 0.4350, 0.0452, 0.0564, 0.0313)
12	NM	PL	0.0213	(0.0398, 0.3763, 0.0199, 0.0259, 0.0257, 0.3431, 0.1693)
13	NS	NL	0.3449	(0.6446, 0.1974, 0.0222, 0.0029, 0.1243, 0.0054, 0.0032)
14	NS	NM	0.7295	(0.6585, 0.0055, 0.0122, 0.0179, 0.0614, 0.0000, 0.2445)
15	NS	NS	0.9325	(0.0903, 0.1514, 0.2291, 0.0008, 0.1997, 0.2286, 0.1001)
16	NS	PS	0.1022	(0.0437, 0.5016, 0.1791, 0.0232, 0.1110, 0.0148, 0.1266)
17	NS	PM	0.5515	(0.1438, 0.0757, 0.5844, 0.1071, 0.0837, 0.0037, 0.0016)
18	NS	PL	0.9984	(0.0612, 0.0087, 0.5805, 0.0614, 0.0519, 0.1757, 0.0606)
19	Z	NL	0.8714	(0.5559, 0.0025, 0.4084, 0.0131, 0.0157, 0.0000, 0.0044)
20	Z	NM	0.9888	(0.3465, 0.0407, 0.0482, 0.1203, 0.2854, 0.1368, 0.0221)
21	Z	NS	0.4516	(0.7366, 0.2634, 0.0000, 0.0000, 0.0000, 0.0000, 0.0000)
22	Z	PS	0.9144	(0.9813, 0.0000, 0.0000, 0.0087, 0.0041, 0.0000, 0.0059)
23	Z	PM	0.0091	(0.2258, 0.3734, 0.0333, 0.0435, 0.1359, 0.0567, 0.1314)
24	Z	PL	0.9684	(0.0205, 0.3635, 0.1206, 0.0136, 0.1268, 0.3166, 0.0384)
25	PS	NL	0.6239	(0.2191, 0.0661, 0.0387, 0.1108, 0.3404, 0.0999, 0.1250)
26	PS	NM	0.4238	(0.4381, 0.1451, 0.0316, 0.0058, 0.1172, 0.0000, 0.2622)
27	PS	NS	0.5263	(0.0921, 0.3888, 0.1175, 0.1501, 0.0346, 0.0882, 0.1287)
28	PS	PS	0.3565	(0.1216, 0.5030, 0.0621, 0.0052, 0.2623, 0.0255, 0.0203)
29	PS	PM	0.8746	(0.3548, 0.1496, 0.3591, 0.0435, 0.0003, 0.0003, 0.0924)
30	PS	PL	0.5817	(0.3637, 0.0541, 0.1098, 0.3181, 0.0282, 0.1189, 0.0072)

31	PM	NL	0.6575	(0.3418, 0.0555, 0.1128, 0.3032, 0.0051, 0.0918, 0.0898)
32	PM	NM	0.7650	(0.7228, 0.0654, 0.0011, 0.0019, 0.1416, 0.0672, 0.0000)
33	PM	NS	0.6408	(0.7320, 0.0633, 0.0013, 0.0128, 0.0387, 0.0547, 0.0972)
34	PM	PS	0.4118	(0.3245, 0.0193, 0.1272, 0.0055, 0.1930, 0.2757, 0.0548)
35	PM	PM	0.8512	(0.5288, 0.0092, 0.0443, 0.0708, 0.2012, 0.1125, 0.0332)
36	PM	PL	0.0752	(0.0239, 0.3601, 0.3785, 0.0009, 0.1242, 0.0568, 0.0556)
37	PL	NL	0.6212	(0.0429, 0.3776, 0.0727, 0.0070, 0.0945, 0.3738, 0.0315)
38	PL	NM	0.7362	(0.0335, 0.3977, 0.0653, 0.0099, 0.0486, 0.0283, 0.4167)
39	PL	NS	0.2774	(0.7959, 0.0370, 0.0113, 0.0140, 0.0055, 0.1274, 0.0089)
40	PL	PS	0.0169	(0.0234, 0.0109, 0.6051, 0.0876, 0.0987, 0.0921, 0.0822)
41	PL	PM	0.0468	(0.1998, 0.0765, 0.0341, 0.0111, 0.1500, 0.3885, 0.1400)
42	PL	PL	0.0081	(0.0033, 0.3734, 0.0487, 0.1960, 0.0130, 0.2415, 0.1241)

Figs.2 and 3 compare predicted and observed outputs, demonstrating accurate leakage detection and alignment with ground truth over time.

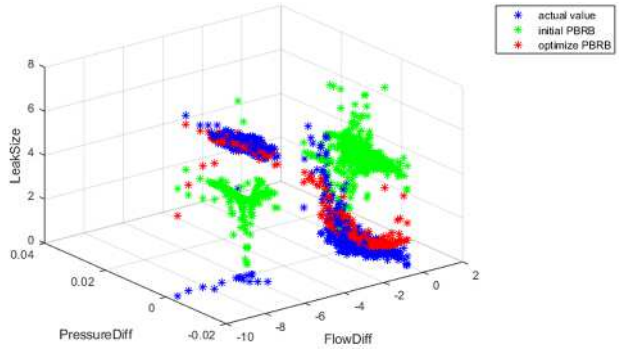

Fig.2 Comparison of model output before and after optimization

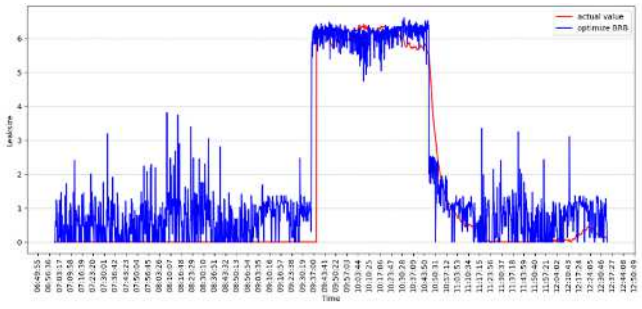

Fig.3 Observation output and output after PBRB training

To assess interpretability improvements, PCA and t-SNE are applied to the activation weight matrix. Fig.4 (PCA) shows clearer clustering boundaries and reduced overlap between rule groups, implying functional differentiation. Fig.5 (t-SNE) reveals tighter local clusters and fewer outliers after optimization. These results confirm that: (1) the model becomes more interpretable post-adjustment; (2) Semantic boundaries between rules are clear; (3) Redundancy is significantly reduced.

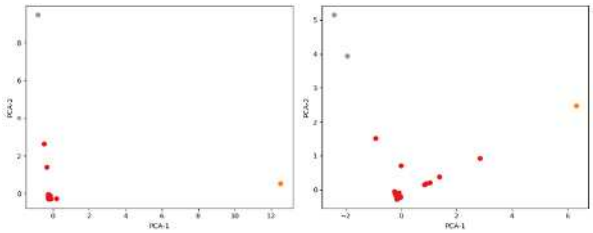

Fig.4 PCA dimension reduction comparison

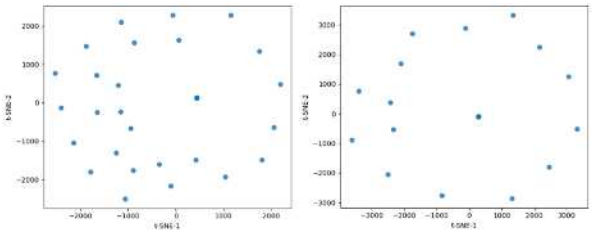

Fig.5 T-SNE dimension reduction comparison

4.2 Comparative study

The comparative experiments were conducted against neural networks [14], fuzzy models [17], and representative BRB optimization approaches such as threshold pruning [18] and interval-based references [19]. As shown in Table 2, the fuzzy model adopts the same parameters as PBRB, and the neural network uses a 32-node hidden layer trained for 500 iterations with a learning rate of 0.001. The proposed PBRB model achieves the lowest MSE among all baselines by mitigating rule explosion and enhancing uncertainty representation.

Table 2 Comparative experiments

Method	MSE
Fuzzy theory	3.7696
Neural network	0.3033
Threshold pruning	0.4266
Interval references	0.4391
PBRB	0.2401
PBRB-DQN	0.1071

5. Conclusion

A novel modeling and optimization framework for fault diagnosis in complex systems is presented in this study, which integrates deep reinforcement learning with the PBRB method. To overcome two major limitations of conventional BRB models: rule explosion and expert knowledge uncertainty, the proposed framework introduces three core innovations: (1) Adaptive reference value adjustment: a Deep Q-Network mechanism dynamically adjusts attributes reference values, based on observed data, effectively compressing the rule base while preserving inference integrity. (2) Multidimensional uncertainty modeling: The optimization process incorporates belief variance and entropy to quantitatively characterize uncertainty within expert knowledge. This facilitates more robust reasoning under ambiguous or incomplete information. (3) Structural assessment and interpretability: A rule activation weight matrix is used in conjunction with PCA and t-SNE to evaluate structural compactness and interpretability before and after optimization.

Empirical validation using a real-world pipeline leak detection dataset demonstrates that the proposed framework significantly improves structural compactness, inference robustness, and prediction accuracy. Compared with traditional BRB models and other baseline methods, the proposed PBRB method shows superior performance in balancing accuracy and interpretability, particularly in uncertain and data-scarce environments. Future work will focus on extending the proposed method to dynamic systems with temporal dependencies and exploring multi-source data fusion strategies to further enhance adaptability and diagnostic performance in real-time industrial scenarios.

References:

[1] Z. Feng, R. Yang, Z. Zhou, and C. Hu, “Trustworthy fault diagnosis method based on belief rule base with multi-source uncertain information for vehicle,” *IEEE Trans. Ind. Electron.*, vol. 71, no. 7, pp. 7947-7956, Jul. 2024.

[2] L. Wen, X. Li, and L. Gao, “A new two-level hierarchical diagnosis network based on convolutional neural network,” *IEEE Trans. Instrum. Meas.*, vol. 69, no. 2, pp. 330-338, Feb. 2020.

[3] Y. Lei, F. Jia, J. Lin, S. Xing, and S. X. Ding, “An intelligent fault diagnosis method using unsupervised feature learning towards mechanical big data,” *IEEE Trans. Ind. Electron.*, vol. 63, no. 5, pp. 3137-3147, May 2016.

[4] M. Chen, N.-C. Xiao, M. J. Zuo, and Y. Ding, “An efficient algorithm for finding modules in fault trees,” *IEEE Trans. Reliab.*, vol. 70, no. 3, pp. 862-874, Sep. 2021.

[5] Xu Li and Weigong Zhang, “An adaptive fault-tolerant multisensor navigation strategy for automated vehicles,” *IEEE Trans. Veh. Technol.*, vol. 59, no. 6, pp. 2815-2829, Jul. 2010.

[6] C. Shao, X. Luo, H. Li, and Z. Tang, “Transient fault detection and failure effect analysis based on design for test and fault tree analysis for automotive chips,” *IEEE Trans. Circuits Syst. Regul. Pap.*, pp. 1-14, 2025.

[7] J. B. Yang, J. Liu, J. Wang, H. S. Sii, and H. W. Wang, “Belief rule-base inference methodology using the evidential reasoning approach - RIMER,” *IEEE Trans. Syst. Man Cybern. Part -Syst. Hum.*, vol. 36, no. 2, pp. 266-285, Mar. 2006.

[8] H. Zhu, J. Zhao, Y. Xu, and L. Du, “Interval-valued belief rule inference methodology based on evidential reasoning-IRIMER,” *Int. J. Inf. Technol. Decis. Mak.*, vol. 15, no. 6, pp. 1345-1366, Nov. 2016.

[9] L. Jiao, T. Denoeux, and Q. Pan, “A hybrid belief rule-based classification system based on uncertain training data and expert knowledge,” *IEEE Trans. Syst. Man Cybern.-Syst.*, vol. 46, no. 12, pp. 1711-1723, Dec. 2016.

[10] X. Cheng, P. Han, W. He, and G. Zhou, “A new interval constructed belief rule base with rule reliability,” *J. Supercomput.*, vol. 79, no. 14, pp. 15835-15867, Sep. 2023.

[11] L. Chang *et al.*, “Disjunctive belief rule base spreading for threat level assessment with heterogeneous, insufficient, and missing information,” *Inf. Sci.*, vol. 476, pp. 106-131, Feb.

2019.

[12] X. Yin, R. Jia, B. Xu, H. Li, H. Zhu, and W. He, "A new state-of-health estimation method for li-ion batteries based on interpretable belief rule base with expert knowledge credibility," *Energy Sci. Eng.*, vol. 11, no. 12, pp. 4722-4736, Dec. 2023.

[13] R. Sun, D. Ouyang, X. Tian, and L. Zhang, "An efficient power set mapping space blocking algorithm for sensor selection in uncertain systems with quantified diagnosability requirements," *Appl. Intell.*, vol. 53, no. 3, pp. 2879-2896, Feb. 2023.

[14] Z. Feng, Z. Zhou, X. Ban, C. Hu, and X. Zhang, "Sensor fault diagnosis and tolerant control based on belief rule base for complex system," *J. Syst. Sci. Complex.*, vol. 36, no. 3, pp. 1002-1023, Jun. 2023.

[15] Z. Feng, W. He, Z. Zhou, X. Ban, C. Hu, and X. Han, "A new safety assessment method based on belief rule base with attribute reliability," *IEEECAA J. Autom. Sin.*, vol. 8, no. 11, pp. 1774-1785, Nov. 2021.

[16] A. Gang and W. U. Bajwa, "FAST-PCA: a fast and exact algorithm for distributed principal component analysis," *IEEE Trans. Signal Process.*, vol. 70, pp. 6080-6095, 2022.

[17] C. Li, Q. Shen, L. Wang, W. Qin, and M. Xie, "A new adaptive interpretable fault diagnosis model for complex system based on belief rule base," *IEEE Trans. Instrum. Meas.*, vol. 71, pp. 1-11, 2022.

[18] H.-C. Liu, L. Liu, and Q.-L. Lin, "Fuzzy failure mode and effects analysis using fuzzy evidential reasoning and belief rule-based methodology," *IEEE Trans. Reliab.*, vol. 62, no. 1, pp. 23-36, Mar. 2013.

[19] H. Wan, Z. Zhang, W. He, M. Li, and H. Zhu, "A new automated interval structure belief rule base-based fault diagnosis method for complex systems," *Nonlinear Dyn.*, vol. 113, no. 8, pp. 8391-8422, Apr. 2025.